β-delayed fission and α decay of ^{178}Tl

V. Liberati,[1] A. N. Andreyev,[2,3] S. Antalic,[4] A. Barzakh,[5] T. E. Cocolios,[6,7,13] J. Elseviers,[6] D. Fedorov,[5] V. N. Fedoseeev,[7] M. Huyse,[6] D. T. Joss,[8] Z. Kalaninová,[4] U. Köster,[9] J. F. W. Lane,[1] B. Marsh,[7] D. Mengoni,[1,10] P. Molkanov,[5] K. Nishio,[3] R. D. Page,[8] N. Patronis,[6,14] D. Pauwels,[6,15] D. Radulov,[6] M. Seliverstov,[1,5,7] M. Sjödin,[7] I. Tsekhanovich,[11,13] P. Van den Bergh,[6] P. Van Duppen,[6] M. Venhart,[6,12] and M. Veselský[12]

[1]*School of Engineering and Science, University of the West of Scotland, Paisley, PA1 2BE, United Kingdom*
[2]*Department of Physics, University of York, York Y010 5DD, United Kingdom*
[3]*Advanced Science Research Center, Japan Atomic Energy Agency (JAEA), Tokai-mura, Naka-gun, Ibaraki 319-1195, Japan*
[4]*Department of Nuclear Physics and Biophysics, Comenius University, 84248 Bratislava, Slovakia*
[5]*Petersburg Nuclear Physics Institute, 188350 Gatchina, Russia*
[6]*Instituut voor Kern-en Stralingsfysica, KU Leuven, University of Leuven, B-3001 Leuven, Belgium*
[7]*CERN, CH-1211 Geneve 23, Switzerland*
[8]*Department of Physics, Oliver Lodge Laboratory, University of Liverpool, Liverpool L69 7ZE, United Kingdom*
[9]*Institut Laue Langevin, 6 rue Jules Horowitz, Grenoble Cedex 9 F-38042, France*
[10]*INFN, Legnaro 35020, Italy*
[11]*Centre d'Etudes Nucleaires de Bordeaux Gradignan, Gradignan Cedex F-33175, France*
[12]*Institute of Physics, Slovak Academy of Sciences, 84511 Bratislava, Slovakia*
[13]*School of Physics and Astronomy, University of Manchester, Manchester M13 9PL, United Kingdom*
[14]*Department of Physics, University of Ioannina, Ioannina 45110, Greece*
[15]*SCK·CEN, Mol 2400, Belgium*

(Received 4 February 2013; published 21 October 2013)

A detailed nuclear-decay spectroscopy study of the neutron-deficient isotope ^{178}Tl has been performed using the highly selective Resonance Ionization Laser Ion Source and ISOLDE mass separator (CERN), which allowed a unique isobarically pure beam of ^{178}Tl to be produced. The first identification of the β-delayed fission of this isotope was made and its probability $P_{\beta\mathrm{DF}}(^{178}\mathrm{Tl}) = 0.15(6)\%$ was determined. An asymmetric fission fragment mass distribution of the daughter isotope ^{178}Hg (populated by the β decay of ^{178}Tl) was deduced based on the measured fission fragment energies. The fine-structure α-decay pattern of ^{178}Tl allowed the low-energy states in the daughter nucleus ^{174}Au to be studied.

DOI: 10.1103/PhysRevC.88.044322 PACS number(s): 23.60.+e, 27.70.+q, 25.85.−w, 29.38.−c

I. INTRODUCTION

β-delayed fission (βDF), discovered in 1965–1966 [1–4], is an exotic two-step process in which a parent (A, Z) nucleus first undergoes β^+/EC decay, populating excited states in the daughter $(A, Z-1)$ isotope. If these states lie in the vicinity of or above the fission barrier of the daughter nucleus, the nucleus then may fission. Clearly, for βDF to occur, the Q_{EC} of the parent nucleus should be higher than or comparable to the fission barrier B_f of the daughter product. In this respect, βDF is a unique tool to study low-energy fission of very exotic nuclei, which do not fission spontaneously from their ground state. The most recent review on βDF is given in Ref. [4].

Recently, the βDF of ^{180}Tl (calculated $Q_{\mathrm{EC}}(^{180}\mathrm{Tl}) - B_f(^{180}\mathrm{Hg}) = 0.63$ MeV; see Table V of [5]) was investigated in detail [6,7], and a surprising asymmetric fission fragment mass distribution of ^{180}Hg (the daughter of ^{180}Tl after β decay) was observed. Furthermore, the βDF probability $P_{\beta\mathrm{DF}}(^{180}\mathrm{Tl}) = 3.2(2) \times 10^{-3}\%$ was deduced.

The present study extends the previous work to ^{178}Tl($Z = 81, N = 97$) for which an even higher $P_{\beta\mathrm{DF}}$ is expected owing to the larger calculated difference of $Q_{\mathrm{EC}}(^{178}\mathrm{Tl}) - B_f(^{178}\mathrm{Hg}) = 1.82$ MeV, which may lead to a higher probability of populating excited states above the fission barrier in ^{178}Hg. To estimate the $Q_{\mathrm{EC}} - B_f$ differences we used theoretical masses [8] and fission barriers [5], as no experimental masses exist for ^{178,180}Tl and the fission barriers have not yet been experimentally determined for ^{178,180}Hg. The use of other mass and fission-barrier models will not change the conclusions of our work.

The first identification of ^{178}Tl was performed at the Fragment Mass Analyzer (FMA) by Carpenter *et al.* [9] by using the complete-fusion reaction ^{103}Rh(^{78}Kr,3n)^{178}Tl. After production and mass separation with FMA, the nuclei of interest were implanted into a 60-μm-thick Double-Sided Silicon Strip Detector (DSSSD), where their α decays were measured. In total, a few tens of α decays of ^{178}Tl were collected (see inset to Fig. 1(a) of [9]) and three αlines were distinguished, but no half-life value was given, see the last column of Table I.

Improved data, with $\sim 10^3$ of $\alpha_1(^{178}\mathrm{Tl})$-$\alpha_2(^{174}\mathrm{Au})$ correlated events (see Figs. 4 and 5 of [10]), were obtained in later work at the Berkeley Gas-Filled Separator (BGFS) by Rowe *et al.* [10]. In their work, ^{178}Tl was produced in the complete-fusion reaction ^{102}Pd(^{78}Kr,pn)^{178}Tl, and after separation with BGFS, the nuclei were implanted into a 300-μm-thick 16-strip Position-Sensitive Silicon Detector (PSSD). Four α-decay transitions were observed, three of them in good agreement with data from [9]; see Table I. Despite using two 50% high-purity germanium (HPGe) detectors in Ref. [10], no γ rays were detected in coincidence with these decays; thus, only

TABLE I. A comparison of α-decay energies E_α, half-life values $T_{1/2}$, measured relative α-decay intensities $I_{\alpha,\mathrm{rel}}$ and deduced reduced α-decays widths δ_α^2 for ^{178}Tl from our measurements and from the earlier data. Note that in Ref. [9] no uncertainties for α-decay energies of ^{178}Tl were reported. Our half-life value for ^{178}Tl is $T_{1/2} = 252(20)$ ms.

Present work					Ref. [10]			Ref. [9]
E_α (keV)	I_α (%)[b]	$I^{\mathrm{b}}_{\alpha,\mathrm{rel}}$	δ_α^2 (keV)[b]	$Q_{\alpha,\mathrm{tot}}$ (keV)	E_α (keV)	Half-life (ms)	$I_{\alpha,\mathrm{rel}}$	E_α (MeV)
6595(10)	24(5)	0.34(7)	10.2(24)	7020(10)	6616(15)	224^{+25}_{-19}	0.23	–
6693(10)	70(4)	1	13.0(17)	7020(10)	6704(5)	247^{+14}_{-11}	1.0	6.71
[6783(10)][a]			–	–	6785(5)	273^{+26}_{-20}	0.30	6.79
6862(10)	6(3)	0.09(5)	0.30(15)	7020(10)	6859(5)	246^{+29}_{-21}	0.17	6.87

[a]Artificial α line owing to the α + conversion electron energy summing in the silicon detector (see text).
[b]The reported intensities and reduced widths in the table and in Fig. 3 were corrected for the effect owing to 6783-keV summing $\alpha + e^-$ line (see text).

a schematic decay pattern for ^{178}Tl was proposed (see Fig. (6) of Ref. [10]). It is worth mentioning that in both studies [9,10], α decays of ^{178}Tl constituted only a small fraction of all α decays registered in the silicon detectors with a much larger number of α decays originating from several dominant p, xn and α, xn reaction channels.

The α decay of the daughter isotope ^{174}Au was previously investigated in the works [10–13]. The most recent work [11] proposed the existence of two α-decaying isomeric states in this nucleus; see Sec. III D. Because their relative excitation energy is not yet known, we denote them as ^{174}Au^{m1} and ^{174}Au^{m2} in the following discussion.

We performed two experiments at the ISOLDE mass separator [14] at CERN (Run I in 2008 and Run II in 2010). A unique combination of the Resonance Ionization Laser Ion Source (RILIS) [15] and the mass separation provided by ISOLDE, allowed a very pure source of ^{178}Tl to be produced and in total $\sim 4.3 \times 10^3$ α decays of ^{178}Tl were detected. The use of HPGe detectors in compact geometry allowed α-γ coincidences to be measured efficiently, which led to a detailed fine-structure α-decay study of this nucleus and unambiguous identification of several new excited states in the daughter nucleus ^{174}Au; see Sec. III A. Furthermore, the first identification of the β-delayed fission of ^{178}Tl was achieved (Sec. IV), which indicated an asymmetric fission fragment mass distribution in the fission of ^{178}Hg, similar to that of ^{180}Hg. Taken together, the data for ^{178,180}Hg firmly establish a new region of asymmetric fission, in addition to the previously known region in actinides. This work is a part of our program to study βDF in the very neutron-deficient isotopes in the Tl-to-Fr region, see, e.g., the recent βDF investigations of ^{186,188}Bi and ^{192,194}At [16,17].

II. EXPERIMENTAL SETUP

A. Production of a pure ^{178}Tl beam at RILIS + ISOLDE

As both experiments used a very similar technique, only a short overview of the most relevant details is provided here. A detailed description of the setup and analysis techniques are given in our papers [6,7,18], which report the analysis of ^{180}Tl data from Run I. In both experiments, the ^{178}Tl nuclei were produced by the 1.5-μA, 1.4-GeV proton-induced spallation reactions of a thick 50 g/cm^2 UC$_x$ target of ISOLDE mass separator at CERN. The thallium atoms produced in the target were selectively ionized to the 1^+ charge state by using the RILIS of ISOLDE [15]. After the ionization and extraction from the target, ^{178}Tl ions were accelerated up to energies of 30 keV in Run I and 50 keV in Run II and mass separated with the ISOLDE High Resolution Separator (HRS) in Run I and with the General Purpose Separator (GPS) in Run II. The ISOLDE mass resolution in both cases ($\Delta M/M \sim$ 2000–5000) was sufficient to avoid completely the contribution from the neighboring thallium isotopes, which are also ionized by the RILIS. Thus, an obvious advantage of this method is that the combination of RILIS + ISOLDE provided a very pure beam of ^{178}Tl with an average yield of $\sim$0.15 atoms/s ($\sim$0.1 atoms/μC).

B. Detection system

In Run I, after the mass separation, the pure 30-keV ^{178}Tl beam passed through the 6-mm-diameter central hole of an annular silicon detector of 300 μm thickness and active area of 450 mm^2. The ^{178}Tl ions were implanted into one of the ten 20 μg/cm^2 thick carbon foils of the Windmill system, described in detail in Ref. [6]. A second circular silicon detector, of 300 μm thickness and active area of 300 mm^2, was installed 2 mm behind the carbon foil. The use of two silicon detectors allowed the measurements of twofold coincident fission fragments, in addition to detection of α decays and singles fission fragments. The total registration efficiency for a single α or fission decay in one of the silicon detectors was 51%, while coincident fission fragments were registered with an efficiency of 16% [7]. To detect γ- and x-ray decays a single Miniball HPGe cluster [19], consisting of three HPGe crystals, was placed at $\sim$1 cm behind the circular silicon detector, outside the vacuum chamber. This experimental setup is extensively discussed in Ref. [7].

In Run II, the 50-keV ^{178}Tl beam was also implanted into carbon foils of the Windmill system. No annular silicon detector was used and the α and fission decays were measured by a single circular silicon detector installed behind the foil, as in Run I. Furthermore, the Miniball cluster was replaced by two HPGe detectors of relative efficiency 90% and 70% placed behind and to the side of the vacuum chamber, respectively. This configuration allowed single-particle decays (α, β, and fission) to be measured efficiently in coincidence with γ decays.

In both experiments the energy range of the silicon detectors was set from ∼200 keV to 100 MeV to allow observation of low-energy conversion electrons, β particles punching through the silicon detector, α decays and fission fragments. The α-decay energy calibration was performed using the well-known α decays of the daughter products of ^{178}Tl decays: ^{178}Hg ($E_\alpha = 6429(4)$ keV [20]) and ^{174}Pt ($E_\alpha = 6039(3)$ keV [21]). An energy resolution of 40 keV [full width at half maximum (FWHM)] was measured for the α decays in the range of 5000–7000 keV in this mode.

A digital data acquisition system was used in both runs. The signals from the silicon and germanium detectors were fed into DGF-4C modules, developed by the XIA company [22]. In a triggerless approach the coincidences were then extracted off-line.

III. RESULTS

A. α decay of ^{178}Tl

In the two experiments, approximately 4.3×10^3 α decays of ^{178}Tl were observed (∼1.9×10^3 in Run I and ∼2.4×10^3 in Run II) in total. A part of the total α-decay energy spectrum measured in the silicon detectors is shown in Fig. 1. Figure 1(a) demonstrates the purity of the ^{178}Tl source as all the observed decays originate either from ^{178}Tl itself, or from its daughter products: ^{174}Au (after α decay) and ^{178}Hg and ^{174}Pt (after β^+/EC decay). This is a clear advantage of the method in comparison with the studies at the FMA [9] and BGFS [10], in which several other isotopes were simultaneously and much more abundantly produced and implanted in the silicon detector.

The four αpeaks seen in Fig. 1(a) at the energies of 6595(10), 6693(10), 6783(10), and 6862(10) keV are attributed to the decay of ^{178}Tl, as discussed below. Within the quoted uncertainties, the measured α-decay energies of ^{178}Tl are in a good agreement with the literature values (see Table I). The second column of Table I provides the experimental intensities of the 6595-, 6693-, and 6862-keV transitions, while their relative intensities, normalized with respect to the 6693-keV line are given in the third column. Our values are comparable with the corresponding values reported (without uncertainties) in Ref. [10].

Anticipating the detailed discussion in Sec. III A2, we mention at this point that the peak at 6783 keV does not represent an actual α decay of ^{178}Tl and results from the α-particle-conversion electron summing in the silicon detector. That is why this artificial α-decay line is shown in brackets in Table I and no intensity value quoted. The measured intensity of this line [(14(3)%] was redistributed to the 6595- and 6693-keV α-decay lines, as described in Sec. III A2. The intensities and reduced widths quoted in Table I were corrected for this effect.

The two-dimensional spectrum in Fig. 1(b) shows the α-γ coincidences, for α-decay events from Fig. 1(a), observed within the time interval of $\Delta T(\alpha - \gamma) \leqslant 600$ ns. Two regions of interest are marked with the rectangles "G1" and "G2" in this spectrum, being the γ rays in coincidence with the 6595- and 6693-keV α decays, respectively. Projections on the E_γ axis from the regions G1 and G2 of Fig. 1(b) are shown in Figs. 2(a) and 2(b), respectively. In addition to the Au$K_{\alpha,\beta}$ x rays at 67–80 keV, the γ rays at 163.0(5), 173.0(5), and 273.0(5) keV are seen in coincidence with α decays of ^{178}Tl.

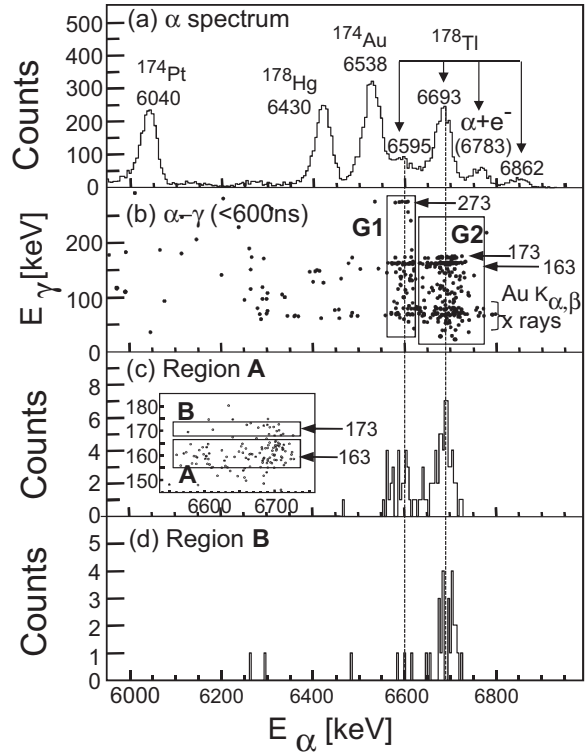

FIG. 1. (a) Part of the α-decay spectrum collected in the silicon detectors, from the combined statistics (Run I and Run II). The α peaks are denoted with their energies in keV and the isotope to which they belong. (b) The α-γ coincidence plot for the α decays from (a), measured within the time interval $\Delta T(\alpha$-$\gamma) \leqslant 600$ ns. Panels (c) and (d) give the projections on the E_α axis from the regions "A" and "B" of the inset to panel (c). The latter shows an expanded part of α decays from panel (b) being in coincidence with the 163- and 173-keV decays.

An expanded part of Fig. 1(b) is shown as an inset to Fig. 1(c), emphasizing the α decays in coincidence with the 163- and 173-keV γ rays. The projections on the E_α axis of the two regions from the inset, which are marked by the rectangles "A" and "B," are shown in Figs. 1(c) and 1(d), respectively.

The α-γ coincident events of 6595-273.0(5) keV seen in Fig. 1(b) has the same total Q_α value $Q_{\alpha,\mathrm{tot}} = Q_\alpha + E_\gamma$ as the 6862-keV decay in Fig. 1(a); see Table I. On these grounds we assign the 6862-keV decay as the full-energy direct transition to the state in ^{174}Au (further called ^{174}Au^{m1} state) which decays by the 6538(10)-keV α decay [10], while the 6595-keV feeds to the new excited state at 273.0(5) keV above the ^{174}Au^{m1} state, as depicted in the decay scheme in Fig. 3. The 6595-keV decay is also in coincidence with the 163.0(5)-keV γ-ray energy [see Figs. 1(c) and 2(a)], which establishes the new excited state at 163.0(5) keV in ^{174}Au^{m1}. This also requires the existence of a 110.0(7)-keV linking transition or a cascade of low-energy transitions between the states at 273 and 163 keV. The nonobservation of such transition(s) can only be explained

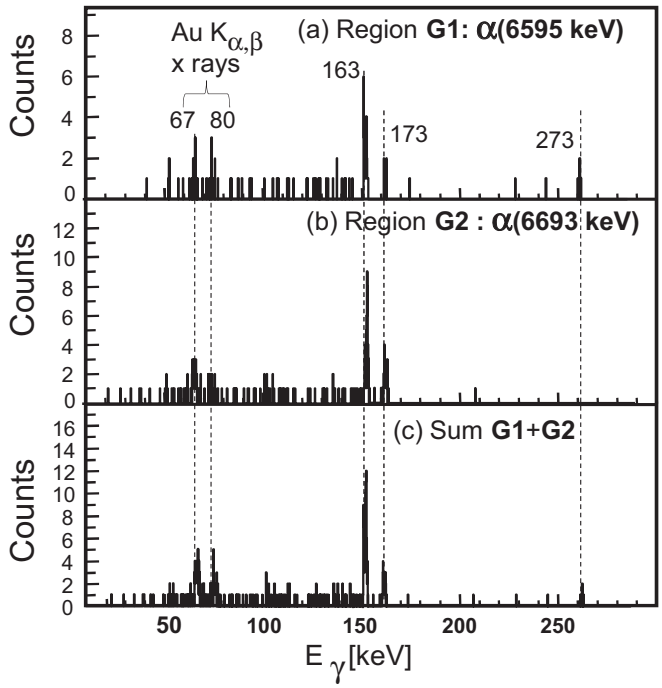

FIG. 2. (a) Projection on the E_γ axis of the region "G1" of the α-γ plot shown in Fig. 1(b); (b) the same, but for the region "G2." The sum of the two projections is displayed in (c). The γ-ray peaks are labeled by their energies in keV. An uncertainty of 0.5 keV is assumed on the γ-ray energy.

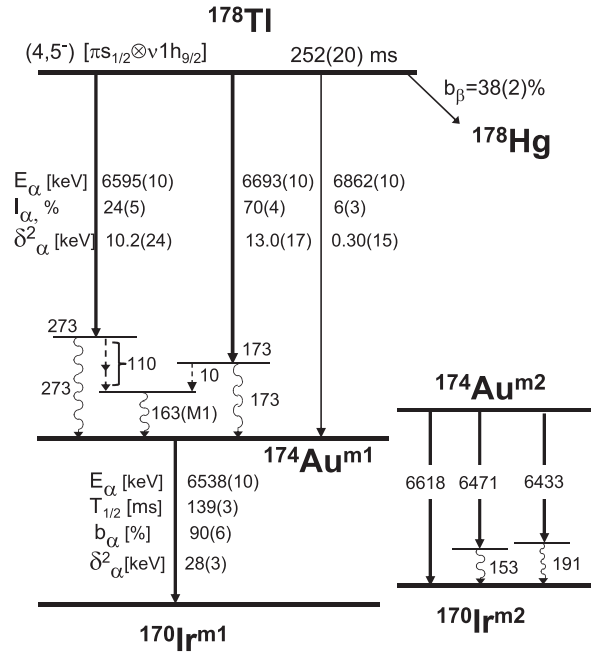

FIG. 3. Decay scheme of ^{178}Tl deduced in this work. The intensities for the 6595- and 6693-keV α decays were corrected to account for the effect of α-e^- summing in the silicon detectors (see text). The decay schemes of two isomers in the daughter nucleus ^{174}Au, compiled from Refs. [10,11], are given to aid the discussion, although the decays from the level labeled "m2" were not seen in our work.

by its strong internal conversion, which is further discussed in Sec. III A2. We also remind the reader that owing to the detection threshold in the silicon detectors (∼200 keV), the respective low-energy conversion electrons could not be seen in our spectra.

Similarly, the α-γ coincident pair of 6693-173.0(5) keV has the same total $Q_{\alpha,\mathrm{tot}}$ value as the 6862-keV decay, which establishes a new excited state at 173.0(5) keV in ^{174}Au^{m1}. This decay path was placed in the scheme as shown in Fig. 3. The 6693-keV decay is also in coincidence with the 163-keV γ ray, see Figs. 1(c) and 2(b). This also requires the existence of a 10.0(7)-keV linking transition between the states at 173 and 163 keV. This transition is shown in Fig. 3 by a dashed line, but is as yet unobserved.

We also considered a scenario in which there is no 10-keV decay, but there are instead two closely lying α decays with energies of 6693 and 6703 keV that contribute to the peak marked as 6693 keV in Fig. 1. In this case, the 6703-keV α decay would feed the 163-keV state directly. However, the analysis of the FWHM values for all the main α-decay peaks in each detector does not indicate that the 6693 line is a doublet, unless the contribution of the 6703-keV decay is small. We therefore discard this scenario.

We also note that there are several 6595-keV-173-keV coincident events in Fig. 1(b) and in Fig. 2(a), which would require a 100-keV γ-ray transition between the states at 273 and 173 keV. However, we interpret these coincidences as arising from the low-energy tail of the strongest 6693-keV α line.

The fact that all three decay paths of ^{178}Tl, namely the direct 6862-keV decay, the 6595-273-keV and 6693-173-keV coincident pairs, have the same $Q_{\alpha,\mathrm{tot}} = 7020(10)$ keV strongly suggests that all of them originate from the same state in ^{178}Tl and finally feed the same state in the daughter ^{174}Au^{m1}. This statement is also supported by the half-life values as deduced from the time behavior of the intensity of the individual α lines, as suggested in Ref. [10] and by our half-life measurements.

1. *Multipolarity of the 163-, 173-, and 273-keV γ rays in ^{174}Au*

As the γ-ray transitions following α decays of ^{178}Tl are prompt, this limits their multipolarity to $E1$, $M1$, or $E2$. Moreover, the intensity ratios of the 163-keV γ ray and the Au$K_{\alpha,\beta}$ x rays in Figs. 2(a) and 2(b) are practically the same (∼1). Because the 163-keV γ ray is the strongest in Figs. 2(a) and 2(b) and as the 173- and 273-keV γ rays are weak in these spectra, this strongly suggests that the Au$K_{\alpha,\beta}$ x rays in these plots originate mainly from the internal conversion of the 163-keV transition. Based on the intensity ratio of $I(163\ \mathrm{keV})/I(\mathrm{Au}K_{\alpha,\beta}\ \mathrm{x\ rays})$ from Fig. 2(b), corrected for the respective difference in the γ-ray detection efficiency, a K-shell conversion coefficient of $\alpha_K(163\ \mathrm{keV}) = 1.7(3)$ was deduced. A comparable value of $\alpha_K(163\ \mathrm{keV}) = 2.0(5)$ could be deduced from the same ratio taken from Fig. 2(a). Both of these values should be considered as upper limits as the the possible conversion of the 173- and 273-keV

transitions could slightly increase the number of Au$K_{\alpha,\beta}$ x rays. Despite this, within the experimental uncertainty, the deduced internal conversion coefficient establishes an $M1$ multipolarity for the 163 keV decay, as the calculated internal conversion coefficients are $\alpha_K(E1) = 0.098, \alpha_K(M1) = 1.48$, $\alpha_K(E2) = 0.28, \alpha_K(M2) = 7.5$ [23].

This also allows a range of possible multipolarities for the 173- and 273-keV transitions to be determined. As most of the observed Au$K_{\alpha,\beta}$ x rays in Figs. 2(a) and 2(b) should be attributed to the 163-keV decay, the multipolarity of the 173-keV decay should be limited to $E1$ [$\alpha_K(E1, \text{calc.}) = 0.084$] or to $E2$ [$\alpha_K(E2, \text{calc.}) = 0.24$] [23]. All other multipolarities for the 173-keV decay should be excluded because they would result in a large excess of observed Au$K_{\alpha,\beta}$ x rays in Fig. 2(a). On similar grounds, the range of possible multipolarities for the 273-keV transition can be established as $E1$, $M1$, or $E2$.

From the intensity ratio of the 173- and 163-keV transitions in coincidence with the 6693-keV α decay, it is very likely that the proposed but unobserved 10-keV transition is of $M1$ multipolarity and the 173-keV transition has $E2$ multipolarity. Any other combination would be incompatible with the observed total transition intensity ratio.

Finally, a comment on the nonobservation of the expected 110-keV transition between the states at 273 and 163 keV should be made. As mentioned above, its nonobservation can be explained only by its strong internal conversion. However, the transition cannot be strongly K-shell converted, as this would result in an excess of expected Au$K_{\alpha,\beta}$ x rays in Figs. 2(a) and 2(b) in comparison with the observed values. Therefore, we tentatively suggest that instead of a single 110-keV transition, a cascade of at least two lower-energy strongly L-shell converted transitions, most probably of $M1$ or $E2$ multipolarity, occurs between the states at 273 and 163 keV. These decays would not have been observed in our spectra because of the strong internal conversion and the reduced γ-ray detection efficiency at such low energies. Importantly, the L-shell conversion will not disturb the observed number of Au$K_{\alpha,\beta}$ x rays. The presence of such a cascade of the lower-energy transitions from the 273-keV state, which effectively competes with the single higher-energy 273-keV decay again favors an $E2$ multipolarity for the 273-keV decay in comparison with the $M1$ assignment. Therefore, we tentatively assign an $E2$ multipolarity for the 273-keV transition.

2. The 6783-keV summing line

An α peak at 6783(10) keV is seen in Fig. 1(a). Based on its energy, this decay would need to feed a new excited state at 81(10) keV in ^{174}Au. However, no such 6783-81 keV α-γ coincidences were observed in Fig. 1(b); instead, weak coincidences are seen with Au$K_{\alpha,\beta}$ x rays (67–80 keV [24]); see Fig. 1(b).

Therefore, we prefer to assign the 6783-keV peak as an artificial "sum" $\alpha + e^-$ peak, resulting from the summing in the silicon detectors of α decays at 6595 keV and/or 6693 keV with the conversion electrons from the coincident 163-, 173-, and 273-keV γ ray transitions. To explain this statement, we consider the case of 6693-163-keV coincidences. As shown above, the 163-keV is quite strongly K-shell converted, the resulting K-shell conversion electron will have an energy of $E_e = E_\gamma(163\,\text{keV})\text{-}B_K(\text{Au}) \sim 82$ keV, where $B_K(\text{Au}) = 80.7$ keV is the K-shell electron binding energy for Au. Such conversion electrons will be fully stopped in the 300-μm-thick silicon detectors used in our experiments. Owing to the close geometry of the silicon detectors relative to the carbon foil, both 6693-keV α decay and 82-keV coincident conversion electron can be registered in the *same* silicon detector, leading to the *full* energy summing of their energies. This results in an artificial α peak with an apparent energy of ~6775(10) keV, in a good agreement with the observed energy of 6783 keV. We note that the internal conversion of the proposed coincident 10-keV γ decay would also produce electrons with a very low energy, which will be fully stopped in the silicon detector. A similar effect will happen for the 173-keV γ decay, for the 6595-273-keV coincidence decay and, more generally, the conversion of the proposed 110-keV transition could also contribute to the summing effect.

As the 163-keV transition is in coincidence with both 6595- and 6693-keV α decays [see Fig. 1(c)], the intensity of both α decays will be influenced by the summing effect. Thus, very approximately, the measured intensity of the summing peak at 6783 keV [14(3)%] should be redistributed between these two α decays in the ratio of approximately of ~1:2, being the ratio of the two peaks in Fig. 1(c). With this procedure, the resulting intensities of the 6595- and 6693-keV α lines become 24(5)% and 70(4)%; see Table I and Fig. 3. These intensities were also used to calculate the respective reduced widths; see Sec. V B.

We also note that the expected presence of a cascade of low-energy L-converted γ transitions (to explain the missing 110-keV transition) could slightly change the above ratio, as the summing owing to these transitions will only influence the 6595-keV decay. However, it is difficult to quantify this effect. We return to the implications of this effect in the Discussion section.

We finally note that such $\alpha - e^-$ summing effects should be even more important in the case of the BGFS experiment [10], in which the nuclei were implanted directly into the 300-μm-thick silicon detector. In case of the FMA experiment [9], the use of a thinner 60-μm-thick DSSSD could weaken the summing effect, but the quality of the spectrum in Fig. 1(a) of Ref. [9] does not allow any conclusions to be drawn in this case.

3. Half-life value of ^{178}Tl

The half-life determination of ^{178}Tl was made by using data from Run I only, as no timing information in the milliseconds-to-seconds range was available in Run II. The grow-and-decay method, described in detail in Ref. [18], was applied for the half-life determination of ^{178}Tl by using its α decay.

The sum of all four transitions in the α-energy interval of 6590–6870 keV of Fig. 1 was used for the half-life analysis. The corresponding time distribution is shown in Fig. 4, which resulted in the half-life value of $T_{1/2} = 252(20)$ ms, which is consistent, within the uncertainty, with the value for the individual 6693-keV decay and also with the literature value

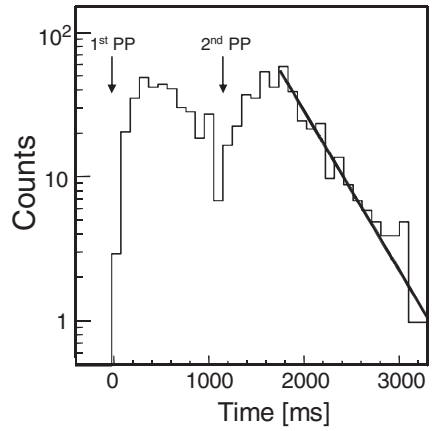

FIG. 4. The sum time distribution for all α decays of ^{178}Tl, determined using as reference the times of two consecutive proton pulses indicated as first PP and second PP in the figure, respectively. See Ref. [18] for the description of the timing system used in the experiment. The decay part of the time distribution was fitted with an exponential function, resulting in a value of $T_{1/2}(^{178}\text{Tl}) = 252(20)$ ms.

of 254^{+11}_{-9} ms [10]. In the following discussions we use our value of 252(20) ms.

B. α- and β-decay branching ratios of ^{178}Tl

The purity of the ^{178}Tl source allowed the first experimental determination of the β- and α-decay branching ratios of this isotope. First of all, no direct production of ^{178}Hg was possible in our experiments, as mercury isotopes cannot be ionized either by surface ionization or by laser ionization tuned to the thallium excitation scheme. This was proved in the measurements with ^{180}Tl, when the ratio between ^{180}Tl and ^{180}Hg was compared with the laser tuned on thallium ionization and with the laser tuned off [18]. Therefore, all α decays of ^{178}Hg observed in Fig. 1(a) are attributed to the β decay of implanted ^{178}Tl.

By comparing the intensities of the parent ^{178}Tl and daughter ^{178}Hg α decays in Fig. 1(a), and by using the ^{178}Hg α-decay branching ratio $b_\alpha = 89(3)\%$ [25], branching ratios of $b_\beta = 38(2)\%$ and $b_\alpha = 62(2)\%$ were deduced for ^{178}Tl. We note that the previously reported estimate of $b_\beta(^{178}\text{Tl}) \sim 47\%$ in Ref. [10] was inferred by comparing the measured half-life value of ^{178}Tl with the calculations within the gross theory of β decay.

Excited levels in ^{178}Hg up to $J^\pi = 20^+$ have been investigated by Kondev *et al*. using the Gammasphere spectrometer coupled to the FMA [20,26]. The low statistics obtained for the β-γ coincidences prevented the identification of γ rays in ^{178}Hg after β decay of ^{178}Tl, so no useful β-γ information was available for ^{178}Tl from the present study.

C. Decay of ^{174}Au

The α decay of the isotope ^{174}Au was previously investigated in Refs. [10–13]. In particular, in the same study of ^{178}Tl at the BGFS [10], a 6538-keV α line with a half-life of 139(3) ms was reported from the state in ^{174}Au with an α-decay branching ratio of 90(6)%.

The latest detailed in-beam and α-decay study of ^{174}Au by Goon [11] claimed identification of the second α-decaying state in ^{174}Au with a complex α-decay pattern and very tentative spin assignments of (9^+). They also proposed a tentative spin assignment of (3^-) to the state decaying by the 6538-keV α decay, seen in earlier studies. For convenience of the discussion we added the decay schemes of both isomers in ^{174}Au to Fig. 3. We also refer the reader to the extensive evaluation [27] in the ENSDF of the ^{174}Au-^{170}Ir-^{166}Re decay chain, which strongly relies on the unpublished data from Ref. [11] and thus should be considered with caution. According to the decay scheme of $^{174}\text{Au}^{m1,m2}$ compiled from [10,11], the low-spin isomer of ^{174}Au is proposed to decay by a single α transition to the (3^-) state in ^{170}Ir, while the decay of the (9^+) isomer in ^{174}Au proceeded via three paths involving either a direct 6618-keV α decay to the (8^+) state in the daughter ^{170}Ir or two α decays observed in coincidence with γ rays: 6471-153 keV and 6433-191 keV. All spin and configuration assignments are tentative and were made based on analogy with the decay sequences of the heavier odd-odd $^{176,178}\text{Au} \rightarrow {}^{172,174}\text{Ir}$ chains, whose spin-parity assignments are often also tentative; see evaluation [27] and the in-beam study of ^{170}Ir in Ref. [28].

As seen in Fig. 1(a), a peak at 6538(10) keV was observed and attributed to the decay of ^{174}Au, which can be produced only after α decay of ^{178}Tl, owing to the mass setting of ISOLDE to mass $A = 178$. The observed energy is in a good agreement with the values of 6547 keV from Ref. [11] and 6538(13) from previous works [10,12,13].

If the high-spin isomer of ^{174}Au was also populated in the α decay of ^{178}Tl, we would expect to see the corresponding 6618-, 6471-, and 6433-keV α decays in Fig. 1(a), but they would be masked by the α decays of ^{178}Tl and ^{178}Hg. However, the nonobservation in our spectra of the 6471-153-keV and 6433-191-keV α-γ coincidences [see Fig. 1(b)], established by Ref. [11], rules out the population of the high-spin isomer in ^{174}Au in our experiment. This provides strong constraints on the possible spin/configuration assignment for ^{178}Tl.

IV. β-DELAYED FISSION OF ^{178}Tl

For the first time the β-delayed fission of ^{178}Tl (fission of ^{178}Hg after β decay of ^{178}Tl) has been identified in this work with eight fission events observed in the region of 40–80 MeV; see Fig. 5(a). One event was measured in Run I and seven events in Run II. We remind the reader that in Run II only one silicon detector was used, so that the observation of coincident fission events was not possible in this run. In Run I two silicon detectors were used, but owing to the fission fragment coincidence efficiency of $\sim$16% [7], no coincident fission events were observed.

Six γ rays were detected in prompt coincidence with these eight fission events. This is in good agreement with a value of $\sim$75% of fission events being in coincidence with γ rays, as seen for the βDF of ^{180}Tl in Refs. [6,7], where a higher statistics sample of 1111 singles fission events was collected using a similar setup with a comparable γ-ray detection efficiency.

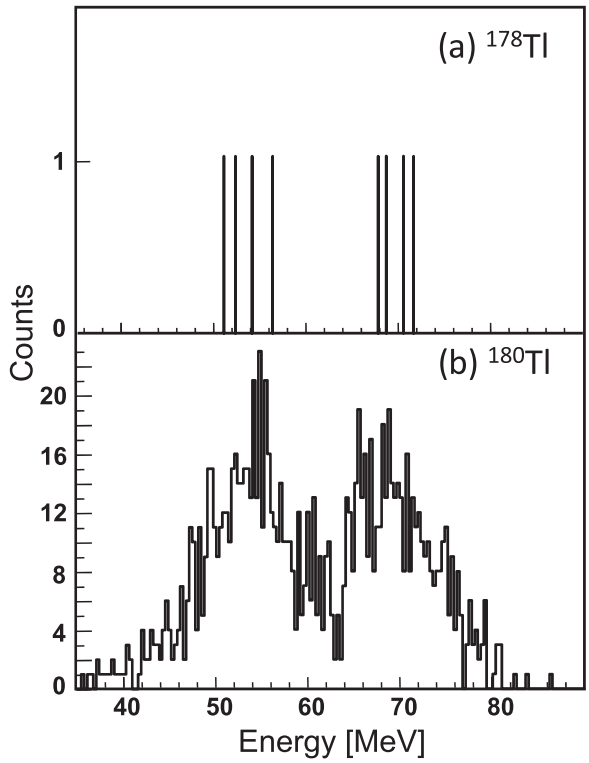

FIG. 5. (a) Energy spectrum for βDF of ^{178}Tl in the fission energy range from the combined statistics (Run I and Run II). (b) Energy spectrum for βDF of ^{180}Tl; data are taken from Refs. [6,7].

In Fig. 5(b), the fission fragment energy spectrum measured for ^{178}Tl is compared to the energy spectrum obtained for βDF of ^{180}Tl [6,7]. Owing to the lack of the fission coincidence events in the study of ^{178}Tl, a proper fission energy calibration of the silicon detectors using the Schmitt calibration method [29,30] was not possible, as it relies on the use of coincidence events for the isotope of interest. Therefore, as a first step, the energy calibration of the silicon detectors in the fission energy region was performed by extrapolating the calibration based on α decays of ^{178}Tl and its daughters from Fig. 1(a) to higher energies. This method obviously suffers from the presence of the pulse height defect in silicon detectors for heavy and relatively slow-moving fission fragments [29,30]. However, by comparing the βDF data for ^{178}Tl and for ^{180}Tl, for which the proper calibration with coincidence fission events was performed in Refs. [6,7], we were able to provide a sufficiently reliable calibration for the eight ^{178}Tl fission events.

For the purpose of this comparison, the βDF spectrum of ^{180}Tl in Fig. 5(b) was also calibrated using the α-energy region of respective α decays of ^{180}Tl. Based on this calibration, the energies of the light and heavy mass peaks in this spectrum are $E_L = 69.4(12)$ and $E_H = 53.5(12)$ MeV, which gives a first-order total kinetic energy of TKE(^{180}Hg) = 122.9(17) MeV, which must be corrected for the pulse height defect. This can be done by comparing this value with TKE(^{180}Hg) = 133.2(14) MeV deduced in Ref. [7] by using the Schmitt method, which accounts for the pulse height defect. Thus, a shift of 10.3(22) MeV can be deduced for ^{180}Hg, owing to the use of the calibration based on α-decay lines.

This value was added to the sum of the energies of $E_L = 69(2)$ and $E_H = 53(2)$ MeV deduced for spectrum of ^{178}Tl from Fig. 5(a). This procedure resulted in TKE(^{178}Hg) = 132(3) MeV, which within the larger uncertainty of our measurement agrees well with the value of TKE(^{180}Hg) = 133.2(14) MeV from Refs. [6,7]. The close similarity of both energy spectra in Figs. 5(a) and 5(b) and of the TKE values, suggests that the fission of both isotopes proceeds via the same mechanism and both nuclides fission asymmetrically with similar fission fragment mass distributions.

The β-delayed fission probability, $P_{\beta\mathrm{DF}}(^{178}\mathrm{Tl}) = 0.15(6)\%$, was deduced from the relation $P_{\beta\mathrm{DF}}(^{178}\mathrm{Tl}) = N_{\beta\mathrm{DF}}(^{178}\mathrm{Tl})/N_{\beta}(^{178}\mathrm{Tl})$, by comparing the number of fission decays $N_{\beta\mathrm{DF}} = 8$ and the number of β decays of ^{178}Tl[$N_{\beta}(^{178}\mathrm{Tl})$]. The latter value is equal to the number of observed α decay of the isotope ^{178}Hg in Fig. 1(a), corrected for its branching ratio of 89(3)% taken from Ref. [25]. The factor of two difference in the detection efficiencies for α particles and fission fragments was also taken into account. It comes from the fact that fission fragments are always emitted in pairs, flying in opposite directions. The measured ratio of number of α decays and fissions, corrected for respective registration efficiencies by the single detector, was $\sim$700. As mentioned in Sec. III B, this method relies on the fact that no direct production of ^{178}Hg is possible in our experiments, thus assuming all ^{178}Hg is produced via β decay of ^{178}Tl.

V. DISCUSSION

A. General systematics of the multiplet states in ^{178}Tl and ^{174}Au

Spectroscopic studies of the odd-odd Tl and Au isotopes are difficult, as even at low excitation energy the level density can be relatively high owing to the coupling of different valence protons and neutrons. Such coupling results in a multitude of rather closely spaced, often isomeric, configurations which have been observed in these nuclei; see, e.g., the previous studies of the heavier odd-odd nuclei $^{188-200}$Tl [31–33]. Moreover, an inspection of the Nilsson diagrams in the region of interest (Fig. 6) shows that the interpretation of the states in ^{178}Tl ($N = 97$) and ^{174}Au ($N = 95$) could be further complicated by the close proximity to the respective Fermi surfaces and a near degeneracy of the $\pi 3s_{1/2}$ and $\pi 2d_{3/2}$ proton orbitals on the one hand and of the $\nu 1h_{9/2}$ and $\nu 2f_{7/2}$ neutron orbitals on the other. If these nuclei become deformed, strong configuration mixing could be further involved. Therefore, the first step in our discussion is the inspection of the known low-lying states in the neighboring odd-A Tl and Au isotopes, which could provide direct information on the lowest proton configurations expected in ^{178}Tl and ^{174}Au, respectively.

Recently, the systematics of the low-lying excited states in odd-A Tl isotopes were reviewed in Fig. 5 of Ref. [35]. That paper, and references therein, are extensively referred to in the following, as well as Fig. 6 of the present paper. All known odd-A isotopes $^{177-209}$Tl are presumed to have spherical ground states with a spin of $I = 1/2^+$ corresponding to the $\pi 3s^{-1}_{1/2}$ proton configuration [35–38]. Excited $3/2^+[\pi 2d^{-1}_{3/2}]$ states are known up to ^{181}Tl ($N = 100$) and typically lie

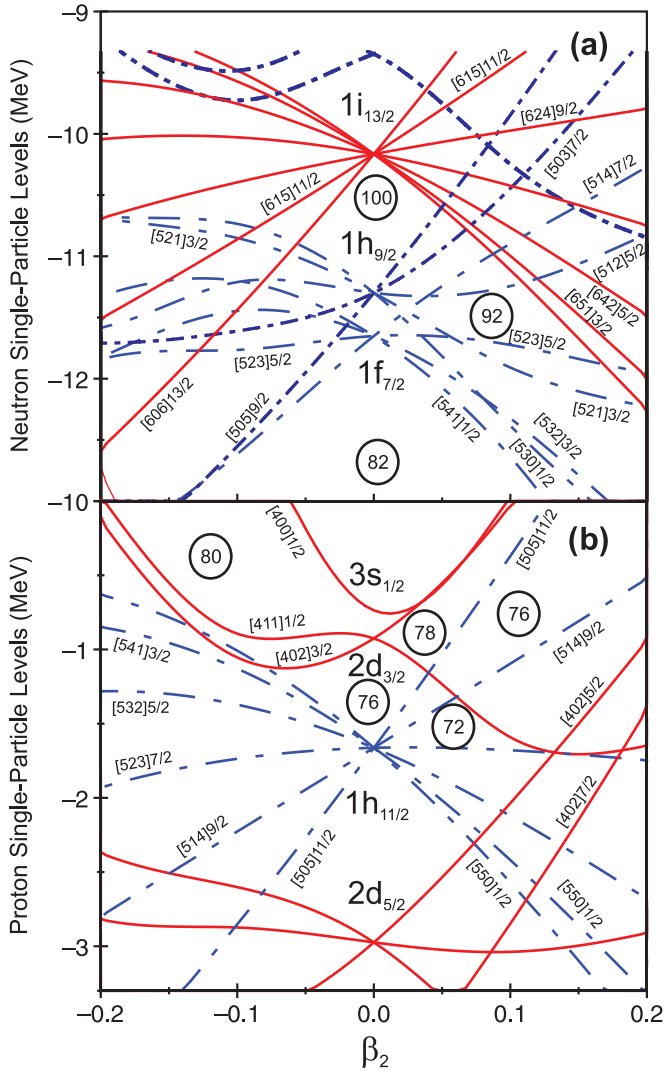

FIG. 6. (Color online) Nilsson orbitals, relevant for the region of ^{178}Tl and ^{174}Au, calculated with a Woods-Saxon potential [34]: (a) for neutrons and (b) for protons.

at a low excitation energy of 250–350 keV. Other possible configurations (where known), such as the $\pi 1h_{11/2}$ or the intruder $\pi 1h_{9/2}$ states, are expected at a much higher energy of at least 800 keV in the vicinity of $N = 97$ [35,37]. Therefore, the spherical $\pi 3s^{-1}_{1/2}$ proton configuration is the most likely candidate to be considered as the proton component for the ground state of ^{178}Tl.

The $\nu 3p_{3/2}$ and $\nu 1i_{13/2}$ neutron configurations play a major role in the Tl nuclei with $A \geqslant 181$ ($N \geqslant 101$); see Fig. 6(a) and Ref. [35]. Correspondingly, in the heavier odd-odd Tl isotopes with $A \geqslant 182$, the lowest-lying states were usually associated with the proton-neutron multiplets as arising from the coupling of the $\pi 3s^{-1}_{1/2}$ or $\pi 1h_{9/2}$ protons with the $\nu 3p_{3/2}$ or $\nu 1i_{13/2}$ neutrons.

In contrast to above, it is expected that the $9/2^-[\nu 1h_{9/2}]$ neutron configuration should become dominant in the lighter Tl isotopes with $N \leqslant 100$. The change is attributable to the complete depletion of the $\nu 1i_{13/2}$ and $\nu 3p_{3/2}$ orbitals lying above the $N = 100$ spherical gap and the creation of a low-lying hole $1h^{-1}_{9/2}$ configuration; see Fig. 6(a). A similar effect was already seen in some of the neighboring odd-A, even-Z nuclei with $N \leqslant 100$, e.g., in ^{179}Pb ($N = 97$) [39], ^{181}Pb ($N = 99$) [40,41], in ^{175,177,179}Hg ($N = 95, 97, 99$) [42–44], and in ^{177}Pt ($N = 99$) [21,44,45].

Therefore, owing to the expected change of the neutron configuration below the neutron number $N = 101$, the $[\pi 3s^{-1}_{1/2} \times \nu 1h_{9/2}]_{4,5-}$ configuration is expected to be the lowest in the odd-odd Tl nuclei with $A \leqslant 180$. This expectation was recently confirmed experimentally by our detailed β-decay study of ^{180}Tl ($N = 99$) [18], in which the spin of $I = (4, 5)$ was proposed for the ground state of this isotope. Most probably, the shape of this state is spherical owing to the sphericity of the underlying proton configuration. The same proton-neutron configuration (or, possibly $[\pi 3s^{-1}_{1/2} \times \nu 2f_{7/2}]_{3,4-}$) was also proposed for ^{176}Tl in Ref. [46]. Based on all of the above arguments, the configuration of $[\pi 3s^{-1}_{1/2} \times \nu 1h_{9/2}]_{4,5-}$ is the most likely for the ground state of ^{178}Tl and is shown in Fig. 3.

A very complex situation is, however, expected for the ground state and the lowest states of ^{174}Au, that can be fed by α decay of ^{178}Tl. This is because the isotope ^{174}Au lies in the middle of the transitional region between possibly weakly deformed or triaxial isotopes ^{175,177}Au on the one hand and nearly spherical isotopes ^{171,173}Au on the other [47].

In our opinion, with the presently available data from all previous studies of ^{170}Ir and ^{174}Au, it is practically impossible to draw definite conclusions on the specific configurations for these nuclei. For a detailed overview of the very complex situation in the $^{174}\text{Au} \rightarrow {}^{170}\text{Ir} \rightarrow {}^{166}$Re chain, we refer the reader to the extensive evaluation of possible proton and neutron configurations in these isotopes given in the Evaluated Nuclear Structure Data File for ^{170}Ir [27]. This thorough evaluation also stresses the multitude and complexity of possible configurations and their strong dependence on the effect of deformation, if it is present in these nuclei, with no unambiguous conclusions drawn. As stated in the above reference, "... The evaluator very tentatively adopts (3^-) and (9^+) for the ^{174}Au isomers." This is based on the *adopted* spin of $I^\pi = (3^-)$ for the daughter ^{170}Ir and the measured hindrance factors for α decays.

To summarize the above overview, we state that while the lowest configuration of ^{178}Tl is most probably $[\pi 3s^{-1}_{1/2} \times \nu 1h_{9/2}]_{4,5-}$, it is very difficult to draw any conclusions on the possible low-lying configurations in ^{174}Au. With the aim of shedding more light on this discussion, in the following section we consider the measured hindrance factors for α decays of ^{178}Tl.

B. Reduced α widths for α decays of ^{178}Tl

Using the measured half-life of 252 ms for ^{178}Tl, the reduced α-decay widths δ^2_α were calculated according to the Rasmussen approach and assuming $\Delta L = 0$ transitions [48] and are presented in Table I. In this procedure the corrected intensities for the 6595- and 6693-keV α-decay lines were used. We stress that even by assuming an extreme scenario and assigning the full intensity of 14% to only one or other of the 6595- or 6693-keV transitions, their reduced width values will not change by a large factor and both of them will still be

in the range of 10–15 keV. These values should be compared to typical reduced α-decay widths of $\delta_\alpha^2 = 40$–90 keV for the well-known unhindered $\Delta L = 0$ α decays of the neighboring ^{177,179}Tl isotopes which proceed between the states with the same spin and parity [36,39].

This comparison shows that the 6862-keV decay is strongly hindered (by at least a factor of ∼100) relative to the unhindered α decays of the neighboring odd-A ^{177,179}Tl isotopes. The hindered nature of the 6862 decay clearly indicates the completely different structure and spin of ^{178}Tl and of the state in ^{174}Au, fed by the 6862-keV decay. Furthermore, the 6862-keV decay is also hindered by at least a factor of ∼25–30 relative to the 6595- and 6693-keV decays of ^{178}Tl, which could possibly indicate the different structure and/or spin of the state in ^{174}Au fed by the 6862-keV decay on the one hand, and of the excited states at 173 and 273 keV on the other.

The 6595- and 6693-keV decays have a comparable strength and appear to be only moderately hindered, by a factor of ∼4–9, relative to the unhindered α decays of the neighboring odd-A ^{177,179}Tl isotopes. This indicates that the structure of the presumed $(4,5)^-$ α-decaying state in ^{178}Tl and of the 173- and 273-keV states should be somewhat similar, but no definitive conclusions in respect of the configurations of the 163-, 173-, and 273-keV excited states in ^{174}Au can be presently drawn.

C. Comparison of fission properties for βDF of ^{178,180}Tl

Figure 7 compares the deduced most probable total kinetic values for ^{178,180}Hg with the known data for the heavier nuclei and also with the Viola fit [49], shown by the black solid line. We refer the reader to the extensive discussion of data for ^{180}Hg in Ref. [7], while here we only point out that both TKE values fit in quite well with the Viola systematics within the experimental uncertainties.

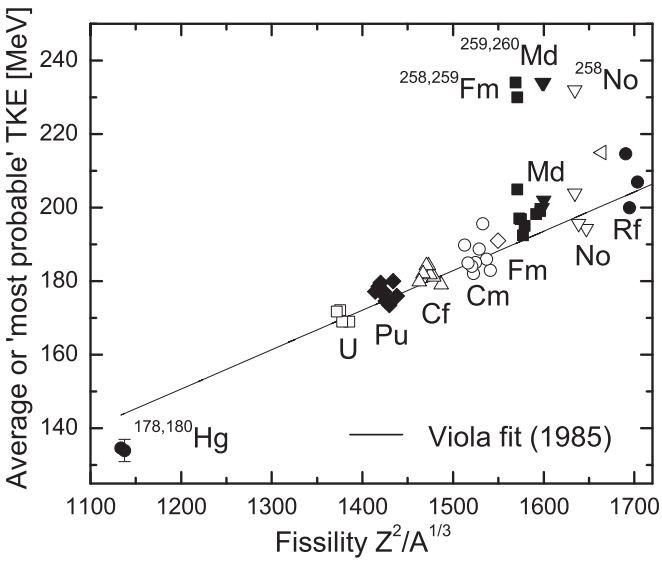

FIG. 7. Systematics of the total kinetic energies as a function of the fissility parameter (Viola systematics) [49]. The Viola fit is shown by the solid line. Owing to their very similar TKE values, ^{178,180}Hg are practically indistinguishable on this plot.

As mentioned earlier, the fission fragment mass distribution for both nuclei is asymmetric, which firmly establishes the new region of asymmetric fission in addition to the well-established region in the heavy actinides and transuranium nuclei. These findings are well reproduced by the recent fission fragment mass yield calculations [50] using the Brownian Metropolis shape-motion treatment [51]. These calculations indeed show very similar shape for mass distributions of ^{178,180}Hg, though the contribution from symmetric fission in ^{178}Hg is predicted to be slightly higher than that in ^{180}Hg.

The deduced βDF probability $P_{\beta\mathrm{DF}}(^{178}\mathrm{Tl}) = 0.15(6)\%$ is about a factor of 46 higher than $P_{\beta\mathrm{DF}}(^{180}\mathrm{Tl}) = 3.2(2) \times 10^{-3}\%$. The increase could indeed be expected owing to the higher calculated difference of $Q_{\mathrm{EC}}(^{178}\mathrm{Tl}) - B_f(^{178}\mathrm{Hg}) = 1.82$ MeV in comparison with $Q_{\mathrm{EC}}(^{180}\mathrm{Tl}) - B_f(^{180}\mathrm{Hg}) = 0.63$ MeV [5]. In a simplified approach, the larger energy difference window should provide more favorable conditions for population of excited states above the top of the fission barrier in ^{178}Hg.

This situation would be in contrast to the case of the fission of ^{180}Hg, where the beyond-barrier fission should be less prominent, owing to the much smaller open window of $Q_{\mathrm{EC}}(^{180}\mathrm{Tl}) - B_f(^{180}\mathrm{Hg}) = 0.63$ MeV. In this case, most fission is expected to occur from the states close to or even below the top of the fission barrier of ^{180}Hg. The fission probability might thus also be determined by the penetrability through the fission barrier (subbarrier fission). To investigate these effects more quantitatively, it would be important to measure in future studies the β-strength function S_β for ^{178,180}Tl.

The knowledge of S_β is also important when attempting to deduce the fission barrier value of the daughter isotopes ^{178,180}Hg from the measured $P_{\beta\mathrm{DF}}(^{178,180}\mathrm{Tl})$, based on statistical model of deexcitation of nuclei. Such an analysis for ^{178,180}Hg was performed in our recent study [52]. Though admittedly somewhat model-dependent, this approach has already been applied in several earlier βDF studies in the transuranium and lead regions [53,54]. By using this framework, and employing several sets of input parameters to check the consistency of the analysis, the fission barriers of ^{178,180}Hg were estimated and were shown to be consistently lower than fission barriers from a range of theoretical approaches; see the detailed discussion in the complementary study [52].

VI. CONCLUSIONS

To conclude, a detailed nuclear spectroscopic study of the neutron-deficient isotope ^{178}Tl has been performed at the ISOLDE mass separator (CERN). Fine-structure α decays of ^{178}Tl gave information on the low-energy excited states in the daughter nucleus ^{174}Au. The first identification of the β-delayed fission of this isotope was made and its probability $P_{\beta\mathrm{DF}}(^{178}\mathrm{Tl}) = 0.15(6)\%$ was deduced. Despite the low number of observed fission events, their measured energy distribution indicated an asymmetric fission fragment mass distribution in the fission of ^{178}Hg, similar to that of ^{180}Hg. Taken together, the data for ^{178,180}Hg firmly establish a new region of asymmetric fission mass split, in addition to the previously known region in the heavier actinides.

ACKNOWLEDGMENTS

We thank the ISOLDE collaboration for providing excellent beams and the GSI Target Group for manufacturing the carbon foils. This work was supported by FWO-Vlaanderen (Belgium), by GOA/2010/010 (BOF KU Leuven), by the IAP Belgian Science Policy (BriX network P7/12), by the European Commission within the Seventh Framework Programme through I3-ENSAR (Contract No. RII3-CT-2010-262010), by a grant from the European Research Council (Contract No. ERC-2011-AdG-291561-HELIOS), by the United Kingdom Science and Technology Facilities Council (STFC), by the Slovak grant agency VEGA (Contracts No. 2/0105/11 and No. 1/0576/13), by the Slovak Research and Development Agency (Contracts No. APVV-0105-10 and No. APVV-0177-11), and by the Reimei Foundation of Advanced Science Research Center (ASRC) of JAEA (Tokai, Japan).

[1] V. I. Kuznetzov and N. K. Skobelev, Yad. Fiz. **4**, 279 (1966); **5**, 271 (1967); **5**, 1136 (1967).
[2] V. I. Kuznetzov and N. K. Skobelev, Phys. Part. Nucl. **30**, 666 (1999).
[3] H. L. Hall and D. C. Hoffman, Annu. Rev. Nucl. Part. Sci. **42**, 147 (1992).
[4] A. N. Andreyev, M. Huyse, and P. Van Duppen, Rev. Mod. Phys. **85**, 1541 (2013).
[5] P. Möller, A. J. Sierk, T. Ichikawa, A. Iwamoto, R. Bengtsson, H. Uhrenholt, and S. Åberg, Phys. Rev. C **79**, 064304 (2009).
[6] A. N. Andreyev *et al.*, Phys. Rev. Lett. **105**, 252502 (2010).
[7] J. Elseviers *et al.*, Phys. Rev. C **88**, 044321 (2013).
[8] P. Möller *et al.*, At. Data Nucl. Data Tables **59**, 185 (1995).
[9] M. P. Carpenter *et al.*, Phys. Rev. Lett. **78**, 3650 (1997).
[10] M. W. Rowe *et al.*, Phys. Rev. C **65**, 054310 (2002).
[11] T.-M. Goon, Ph.D. thesis, The University of Tennessee, Knoxville, 2004.
[12] J. R. H. Schneider *et al.*, Z. Phys. A **312**, 21 (1983).
[13] R. D. Page *et al.*, Phys. Rev. C **53**, 660 (1996).
[14] E. Kugler, Hyperfine Interact. **129**, 23 (2000).
[15] V. N. Fedosseev *et al.*, Rev. Sci. Instrum. **83**, 02A903 (2012).
[16] J. F. W. Lane *et al.*, Phys. Rev. C **87**, 014318 (2013).
[17] A. N. Andreyev *et al.*, Phys. Rev. C **87**, 014317 (2013).
[18] J. Elseviers *et al.*, Phys. Rev. C **84**, 034307 (2011).
[19] J. Eberth *et al.*, Prog. Part. Nucl. Phys. **46**, 389 (2001).
[20] F. G. Kondev *et al.*, Phys. Rev. C **61**, 011303 (1999).
[21] Evaluated Nuclear Structure Data File (ENSDF), http://www.nndc.bnl.gov/ensdf
[22] http://www.xia.com/
[23] T. Kibédi *et al.*, Nucl. Instrum. Methods Phys. Res., Sect. A **589**, 202 (2008); conversion coefficients calculator BrIcc v2.2a, http://wwwrsphysse.anu.edu.au/nuclear/bricc/.
[24] R. B. Firestone *et al.*, *Table of Isotopes*, 8th ed. (Wiley & Sons, New York, 1999).
[25] M. Venhart *et al.*, Eur. Phys. J. A **48**, 7 (2012).
[26] F. G. Kondev *et al.*, Phys. Rev. C **62**, 044305 (2000).
[27] C. M. Baglin, Nucl. Data Sheets **96**, 611 (2002); and update of ENSDF (2008).
[28] B. Hadinia *et al.*, Phys. Rev. C **76**, 044312 (2007).
[29] H. W. Schmitt, W. E. Kiker, and C. W. Williams, Phys. Rev. **137**, B837 (1965).
[30] E. Weissenberger *et al.*, Nucl. Instrum. Methods Phys. Res., Sect. A **248**, 506 (1986).
[31] J. Van Maldeghem and K. Heyde, Fizika **22**, 233 (1990).
[32] A. J. Kreiner, C. Baktash, G. Garcia Bermudez, and M. A. J. Mariscotti, Phys. Rev. Lett. **47**, 1709 (1981).
[33] M. Huyse *et al.*, Phys. Lett. B **201**, 293 (1988).
[34] S. Cwiok, J. Dudek, W. Nazarewicz, W. Skalski, and T. Werner, Comp. Phys. Commun. **46**, 379 (1987).
[35] A. N. Andreyev *et al.*, Phys. Rev. C **80**, 024302 (2009).
[36] G. L. Poli *et al.*, Phys. Rev. C **59**, R2979 (1999).
[37] A. N. Andreyev *et al.*, Phys. Rev. C **87**, 054311 (2013).
[38] K. Heyde and J. L. Wood, Rev. Mod. Phys. **83**, 1467 (2011).
[39] A. N. Andreyev *et al.*, J. Phys. G: Nucl. Part. Phys. **37**, 035102 (2010).
[40] A. N. Andreyev *et al.*, Phys. Rev. C **80**, 054322 (2009).
[41] M. P. Carpenter, F. G. Kondev, and R. V. F. Janssens, J. Phys. G: Nucl. Part. Phys. **31**, S1599 (2005).
[42] D. O'Donnell *et al.*, Phys. Rev. C **79**, 051304(R) (2009).
[43] D. G. Jenkins *et al.*, Phys. Rev. C **66**, 011301(R) (2002).
[44] F. G. Kondev, Nucl. Data Sheets **98**, 801 (2003).
[45] A. Melerangi *et al.*, Phys. Rev. C **68**, 041301(R) (2003).
[46] H. Kettunen *et al.*, Phys. Rev. C **69**, 054323 (2004).
[47] F. G. Kondev *et al.*, Phys. Lett. B **512**, 268 (2001).
[48] J. O. Rasmussen, Phys. Rev. **113**, 1593 (1959).
[49] V. E. Viola, K. Kwiatkowski, and M. Walker, Phys. Rev. C **31**, 1550 (1985).
[50] P. Möller, J. Randrup, and A. J. Sierk, Phys. Rev. C **85**, 024306 (2012).
[51] J. Randrup and P. Möller, Phys. Rev. Lett. **106**, 132503 (2011).
[52] M. Veselský *et al.*, Phys. Rev. C **86**, 024308 (2012).
[53] A. Staudt, M. Hirsch, K. Muto, and H. V. Klapdor-Kleingrothaus, Phys. Rev. Lett. **65**, 1543 (1990).
[54] A. N. Andreyev *et al.*, Phys. Lett. B **312**, 49 (1993).